Applied Physics Letters

Experimental demonstration of externally driven millimeter-wave particle accelerator structure

Cite as: Appl. Phys. Lett. **117**, 073502 (2020); https://doi.org/10.1063/5.0011397
Submitted: 20 April 2020 . Accepted: 29 July 2020 . Published Online: 18 August 2020

Mohamed A. K. Othman, Julian Picard, Samuel Schaub, Valery A. Dolgashev, Samantha M. Lewis, Jeffery Neilson, Andrew Haase, Sudheer Jawla, Bruno Spataro, Richard J. Temkin, Sami Tantawi, and Emilio A. Nanni

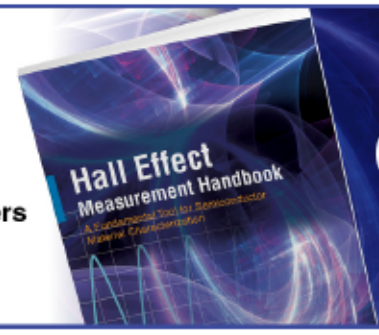

AIP Publishing

Applied Physics Letters ARTICLE scitation.org/journal/apl

Experimental demonstration of externally driven millimeter-wave particle accelerator structure

Cite as: Appl. Phys. Lett. **117**, 073502 (2020); doi: 10.1063/5.0011397
Submitted: 20 April 2020 · Accepted: 29 July 2020 ·
Published Online: 18 August 2020

Mohamed A. K. Othman,[1,a)] Julian Picard,[2] Samuel Schaub,[2] Valery A. Dolgashev,[1] Samantha M. Lewis,[1] Jeffery Neilson,[1] Andrew Haase,[1] Sudheer Jawla,[2] Bruno Spataro,[3] Richard J. Temkin,[2] Sami Tantawi,[1] and Emilio A. Nanni[1,b)]

AFFILIATIONS

[1]SLAC National Accelerator Laboratory, Stanford University, Menlo Park, California 94025, USA
[2]Massachusetts Institute of Technology, Cambridge, Massachusetts 02139, USA
[3]INFN-LNF, Frascati, Rome 00044, Italy

[a)]**Author to whom correspondence should be addressed:** mothman@slac.stanford.edu
[b)]nanni@slac.stanford.edu

ABSTRACT

We report the experimental demonstration of a mm-wave electron accelerating structure powered by a high-power rf source. We demonstrate reliable coupling of an unprecedented rf power—up to 575 kW into the mm-wave accelerator structure using a quasi-optical setup. This standing wave accelerating structure consists of a single-cell copper cavity and a Gaussian to TM_{01} mode converter. The accelerator structure is powered by 110 GHz, 10-ns long rf pulses. These pulses are chopped from 3 ms pulses from a gyrotron oscillator using a laser-driven silicon switch. We show an unprecedented high gradient up to 230 MV/m that corresponds to a peak surface electric field of more than 520 MV/m. We have achieved these results after conditioning the cavity with more than 10^5 pulses. We also report preliminary measurements of rf breakdown rates, which are important for understanding rf breakdown physics in the millimeter-wave regime. These results open up many frontiers for applications not only limited to the next generation particle accelerators but also x-ray generation, probing material dynamics, and nonlinear light-matter interactions at mm-wave frequency.

Exploring new radio frequency (rf) particle accelerator technologies in the mm-wave regime is stimulated by a promise of high accelerating gradient and efficiency for many applications.[1] Indeed, GeV/m acceleration may be attained at mm-wave and subterahertz (THz) frequencies, leveraged by the extremely high shunt impedance that scales as $f^{1/2}$.[1] It is known that cavities with shorter pulses sustain high accelerating gradients. The filling time τ of a cavity scales as $\tau \propto f^{-3/2}$, creating the opportunity for mm-wave accelerators at repetition rates on the order of kHz at high gradients.[2] Indeed, accelerators operating at mm-wave frequencies were considered for linear colliders[3,4] and could be potentially useful in many applications, such as charged particle therapy,[5] compact x-ray free-electron lasers (XFELs),[6] and ultrafast electron diffraction (UED).[7,8]

Advancements of mm-wave accelerator technologies are contingent on the development of efficient high power rf sources. Traditionally, accelerating structures are powered by rf sources (e.g., klystrons) that do not produce the required peak power in the subterahertz range. Attempts to realize high-field subterahertz radiation for electron acceleration previously relied on beam-driven metallic[9] or dielectric[10–13] structures. These earlier studies highlighted challenges in this regime such as fabrication errors[14] and beam-induced damage.[9] On the other hand, laser-driven sources that down-convert the optical regime to subterahertz frequencies are rapidly developing in an effort to fill the THz gap.[15] These laser driven sources generate single- and multi-cycle picosecond pulses with μJ energies.[16,17] They may enable all-optical photoinjectors,[18] deflectors,[19] accelerators,[2,20–22] and bunch compressors[23–25] for ultrafast applications.

Practically, to reach the promised high gradient at mm-waves, nanosecond-scale few-mJ rf pulses are required. So far, these rf parameters may be only realized using mm-wave gyrotrons.[26–29] These are vacuum tubes capable of producing megawatt peak powers with microsecond long pulses[29] or even CW.[28] In this work, we demonstrate a unique approach to power accelerator structures using a megawatt gyrotron rf source. Then, we utilize a laser-driven semiconductor switch to power the accelerating structure with nanosecond scale rf pulses.

The operating gradient of any rf accelerator is limited by rf breakdowns induced by pulsed surface heating and field emission. Over time, the occurrence of breakdowns reduces with the number of pulses, and this process is referred to as conditioning.[30–32] The number of pulses required to condition the cavity depends on many factors including material properties, surface preparation, and geometry of the cavity. It is also known that rf breakdown statistics are associated with the peak electric and peak magnetic fields as well as the peak Poynting vector.[33] Extensive statistical analyses of rf breakdown were performed in normal conducting accelerating structures at microwave frequencies.[30–38]

For instance, CERN's Compact Linear Collider (CLIC) prototype microwave structures[32,37,39] commonly achieve peak gradients of about 100 MV/m. These gradients can be reached only after conditioning the accelerator structures with more than 10^7 pulses to avoid damage from extensive breakdowns and field emissions. After about 10^8 pulse, the breakdown probability at 100 MV/m tends to drop below 10^{-6} per pulse.[32,37] Here, we show that in the mm-wave regime, accelerator structures can reach a gradient of 100 MV/m after only 10^4 pulses and 230 MV/m with only 10^5 pulses. This peak gradient is only limited by the available rf power in our experiment.

Previously, the only measurements of high gradients and rf breakdowns at mm-wave frequencies were performed in beam-driven accelerating structures.[9,40,41] The gradients achieved in these beam-driven structures depended on the geometry and frequency. Unlike the externally driven regime, beam-driven structures[9,40,41] sustained significantly higher surface electric fields for the same gradient. For example, at 122 GHz, the peak surface electric field was about 570 MV/m, and the accelerating mode gradient was about 36 MV/m[40] with a breakdown probability of 6×10^{-2} per pulse. These breakdown rates are achieved with less than 10^6 pulses and were likely influenced by the driving electron bunch and its halo.[9,40,41] Such work emphasized the need for an investigation of high gradient mm-wave accelerator performance under external excitation. In this Letter, we also show preliminary measurement of the breakdown rate of a mm-wave single cell structure at 110 GHz powered by nanosecond scale rf pulses, after similar conditioned with more than 10^5 pulses.

Another challenge toward achieving high-gradient performance at mm-wave frequencies is the precision fabrication and assembly of the accelerating structure. Leveraging state-of-the-art fabrication techniques, we have utilized a split-cell diffusion-bonding technique to assemble the accelerator structure.

We have designed a mm-wave accelerating structure consisting of three coupled cavities and operating in the π-mode. The outer two cavities have a radius of 1.16 mm, while the central cavity's radius is slightly reduced to 1.14 mm. This renders that the peak on-axis field in the central cavity is twice as high as that in the neighboring cells.[31,42] The purpose was to ensure that most of the rf breakdowns occur in the central cavity, since the peak surface fields will also be much lower in the two outer cavities. All cavities are 1.36 mm long. The cell's electric and magnetic fields are shown in Fig. 1(a). The rf properties of the accelerating structure are primarily dictated by the a/λ ratio, where a is the radius of the iris aperture and λ is the free space wavelength. In our design, we have $a/\lambda = 0.105$, similar to 11.424 GHz structures allowing for a direct comparison,[20] with $a = 0.286$ mm. The cavity is designed to achieve 310 MeV/m of steady-state acceleration gradient for 600 kW of dissipated rf power.[42] The shunt impedance of the central cell is 362 MΩ/m, the electric field peak-to-gradient ratio is 2.27, and the peak magnetic-to-electric field ratio (normalized by free space impedance) is 1.04. These design values are obtained by modeling the rf structure with the commercial finite element code HFSS by Ansys. The cavity is connected to a 0.66 mm radius beam pipe for the field emission measurement. The beam pipe is coupled to a WR-8 waveguide port for probing cavity fields.

RF power was coupled to the cavity through the TM_{01} circular waveguide mode, and the waveguide radius is 1.18 mm. Since the high-power pulse is transported from the gyrotron in a fundamental Gaussian beam, the accelerator structure is fed with a tapered Gaussian horn. The Gaussian beam is focused onto a 15 mm diameter circular aperture of a smooth-walled horn with an ~4.5 mm beam waist. The horn converts a Gaussian mode into the TE_{11} mode of a circular waveguide with ~99% efficiency. Following the Gaussian converter is a TE_{11} to TM_{01} mode converter, which includes 90° bend with a 5.23 mm radius. The mode converter has a 97% power conversion efficiency and large bandwidth exceeding 2 GHz.

The accelerating structure was fabricated from two halves of oxygen-free copper, which were aligned and diffusion-bonded. Several prototypes of the structure were fabricated to test the impact of the diffusion-bonding on the rf parameters of the cavity.[42] The submillimeter scale features here are sensitive to fabrication and assembly errors.

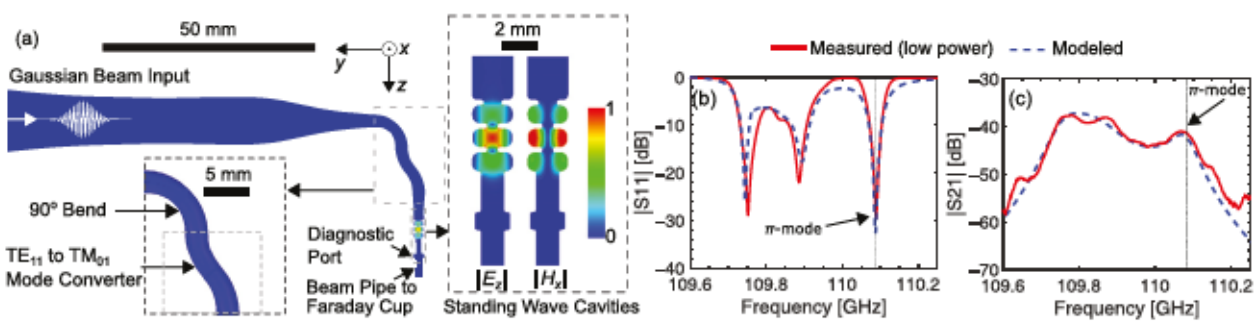

FIG. 1. (a) Rf design of a single-cell mm-wave accelerating structure consisting of the mode converter and the standing-wave cavity showing the normalized accelerating π-mode field profile. The S-parameters (b) S11 and (c) S21 of the mm-wave cavity measured using a quasi-optical setup, showing good agreement with the rf model in the π-mode transmission resonance.

Thus, very strict tolerances were placed during the fabrication and alignment of the two halves. We also found that the cavity frequency tends to slightly increase from pre-bonding to post-bonding, and this shift is considered prior to manufacturing the final high power structure.

The structure was then assembled with a high-power rf window and a dielectric lens, which focuses the Gaussian beam onto the horn aperture. The diagnostic waveguide has its own rf window. The vacuum inside the structure was kept under 10^{-9} Torr. A Faraday cup is connected to the beam pipe to collect field-emitted currents.

Low power, two-port rf measurements of the assembled cavity were performed using a mm-wave vector network analyzer. A Gaussian beam launcher excites the structure as port 1 and a rectangular waveguide as port 2. Figures 1(b) and 1(c) show the results of a measured frequency sweep of the S-parameters as well as simulation results. Three resonances corresponding to the 0, $\pi/2$, and π modes are seen in Figs. 1(b) and 1(c). The π mode resonance is found to be at ~110.08 GHz at about 20 °C (room temperature) with a loaded Q of about 1600. In the S21 measurement, the resonance shows up as a shallow peak of about −41 dB, in very close agreement with the simulations. This also confirms that the horn and mode converter operate within the required bandwidth and efficiency.

The high-gradient experimental setup is shown in Fig. 2(a). The rf source is a 110 GHz megawatt gyrotron that generates 3 μs long rf pulses with a peak power up to 1.25 MW, with a repetition rate of 1 Hz.[43] It is operated at a $TE_{22,6}$ cavity mode with a nominal voltage of 96 kV and a current of 40 A. The generated rf pulses are then transported in a corrugated waveguide that couples the power into a free-space Gaussian mode into the accelerating structure. A quasi-optical attenuator adjusts the forward power toward the accelerating structure, and a quasi-optical ferrite isolator protects the gyrotron from reflections. Overall, there is about 2 dB loss in the high-power rf path that limits the input power to the accelerating structure to about 600 kW.

The 3 μs gyrotron pulses would cause excessive pulsed surface heating in the accelerating cavity, and thus the cavity would require shorter nanosecond-long pulses. To obtain a shorter rf pulse, we have utilized a semiconductor laser-driven switch.[44,45] A 387 μm thick Si wafer illuminated by an intense neodymium-doped yttrium aluminum garnet (Nd:YAG) laser pulse is used as a reflector. The Nd:YAG laser wavelength is 523 nm, the duration is 6 ns, and the pulse energy is 230 mJ. Such a laser pulse impinging on the wafer, which is otherwise transparent at 110 GHz, raises the conductivity of Si due to the generation of charged carriers through photoconductivity until it becomes a reflector with more than 75% reflectivity and redirects the microwaves toward the accelerator.[44,45] The rf pulse length generated from this setup is about 10 ns long and is limited by the carrier recombination rate of silicon[46,47] with the maximum rf pulse energy of about 11 mJ.

The frequency of the gyrotron rf pulses has to coincide with the resonance frequency of the structure's π-mode. Our gyrotron has limited frequency tuning at the peak output power. Therefore, temperature tuning of the cavity using a chiller is employed in order to match the frequency of the π-mode to the gyrotron frequency. This way, the accelerating gradient can be maximized at a fixed power level. In our setup, the frequency tuning range was about 40 MHz and the optimal operating temperature for frequency matching is found to be about 9 °C.

We measured the rf waveforms for each rf pulse: the forward power, the reflected power, and the transmitted power through the diagnostic waveguide. These rf pulses are measured using calibrated mm-wave Schottky diode detectors with sub-ns rise time. We measured field-emitted currents existing at the end of the beam pipe with a Faraday cup. All waveforms are recorded using a 4 gigasample/second oscilloscope. The frequency of the rf pulse is measured with a heterodyne receiver.[29]

Prior to high-power operation, we align the structure to the high-power beam and then calibrate the forward and transmitted power into the structure with our initial low power measurements. An example of an rf pulse at a peak power of 570 kW is shown in Figs. 2(b)–2(d). We note that the measured reflected power is not calibrated [shown in Fig. 2(e) in arbitrary units].

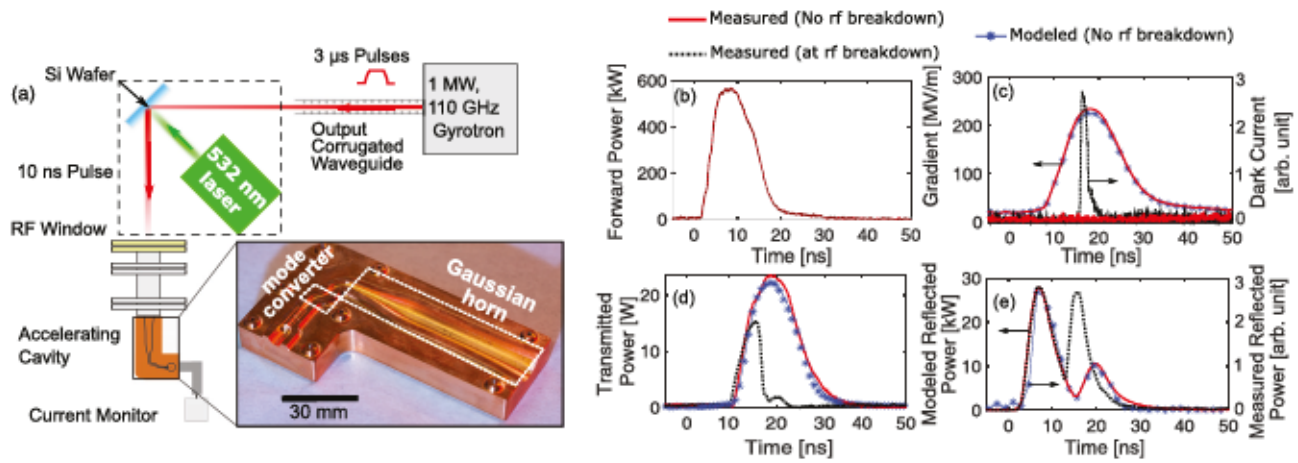

FIG. 2. (a) High-gradient mm-wave accelerating cavity test setup. Example of an rf pulse coupled to the cavity at a peak power of 570 kW, (b) measured forward power into the structure, and (c) the time dependent accelerating gradient and Faraday cup current. (d) Power transmitted through the diagnostic waveguide and (e) reflected power. Dotted lines in (c)–(e) designate an rf breakdown event.

We have used the measured S-parameters to model the cavity transient fields. The modeled time-domain response of the accelerating structure is also superimposed in Figs. 2(b)–2(e). The transmitted power agrees well with our rf model as seen in Fig. 2(d). At the peak input power of 570 kW and pulse length of 11 ns, the peak accelerating gradient is about 230 MV/m as shown in Fig. 2(c). The peak energy gain of a relativistic electron bunch at this gradient is estimated to be about 0.31 MeV from the central cell.

The peak accelerating gradient that can be established in the cavity depends on the rf pulse length, and, therefore, it is important to characterize the pulse length statistics to ensure stable gradient from shot to shot. The forward as well as transmitted pulse full-width half-maximum (FWHM) vs peak forward power is shown in Fig. 3(a). Data shown in Fig. 3 are taken for all the recorded rf pulses except the ones that experience shortening due to rf breakdowns. The FWHM of the forward power is stable and tends to slightly increase with increasing power. This increase in FWHM could be attributed to the rf-driven enhancement of photocarriers in the Si wafer. (More details are in given in Ref. 44.) The ratio between the transmitted and forward pulse FWHM is 1.13 ± 0.03 and that also agrees well with the rf model based on the calculated filling time of the cavity. The accelerating gradient vs forward power together with calculated peak pulse surface heating is also shown in Fig. 3(b). The peak accelerating gradient also demonstrates shot to shot stability and follows a square law fitting with the forward power P in kW, given by $E_{acc} \sim 9.63\sqrt{P}$ [MV/m].

We also show the pulsed surface heating from the rf surface currents on the cavity walls. Pulsed heating is a transient effect[48] and does not impact the frequency or the quality factor of the cavity up to the peak gradient, within the precision of our measurements. Also, the time-average thermal load from the dissipated rf power in the cavity is negligible for such a low pulse repetition rate of 1 Hz, with active temperature-regulated cooling. In our experiment, the peak pulsed surface heating is estimated to be less than 40 °C at the highest power level as seen in Fig. 3(b). From our pervious experiments on damage due to pulsed heating,[34] we expect no surface damage below 50 °C. This damage onset at a peak temperature rise of 50 °C could be reached at a gradient in excess of 260 MV/m.

One of the main goals of our experiment is the study of the physics of vacuum rf breakdown. We observe rf breakdowns as major changes occur to the rf waveforms as follows: (i) transmitted pulse shortening, (ii) sudden jump in the reflected power, and (iii) a short burst of Faraday cup current, as seen from Figs. 2(d) and 2(e). During this experiment, the forward power is gradually adjusted while closely monitoring the breakdown rate at a given power level, see Fig. 4(a). Trigger breakdowns, which are the first in a breakdown chain, are also recorded.[31,33,49]

The rf pulses are collected in sets of 10^3 shots. After a breakdown occurs, pulsing is interrupted for 8 s. This protects the cavity from the damage caused by consecutive breakdowns and ensures that the vacuum level is kept at 10^{-9} Torr. We increase the power when the breakdown rate is below 1%, i.e., less than 10 breakdowns per 10^3 shots. At the end of each day during the experiment, power is lowered by 25% to ensure that breakdown rates are improving. A timeline for testing is depicted in Fig. 4, showing the forward power in Fig. 4(a), the gradient and peak surface fields in Fig. 4(b), and accumulated breakdowns and peak Faraday cup current in Fig. 4(c). Over the course of 10^5 shots, we have seen that the cavity has been rapidly processing up to an accelerating gradient of 230 MV/m. We were able to

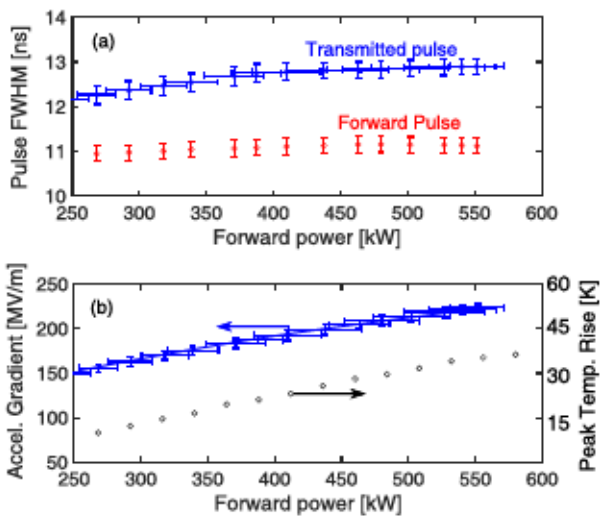

FIG. 3. Stability of gyrotron pulses feeding the accelerating cavity vs different gyrotron powers. (a) Measured FWHM of the forward and transmitted pulses vs forward power, (b) measured field gradient and calculated peak temperature rise due to pulse surface heating vs forward power. The peak accelerating gradient scales with the forward power P in kW as $E_{acc} \sim 9.63\sqrt{P}$ [MV/m], while the temperature rise scales as $131.32\,(E_{acc}/Z_0)^2$, where Z_0 is the free space impedance. The vertical error bars represent rms errors in measurements for a fixed forward power setting. The horizontal error bars are only shown for the transmitted power in (a) and the acceleration gradient in (b).

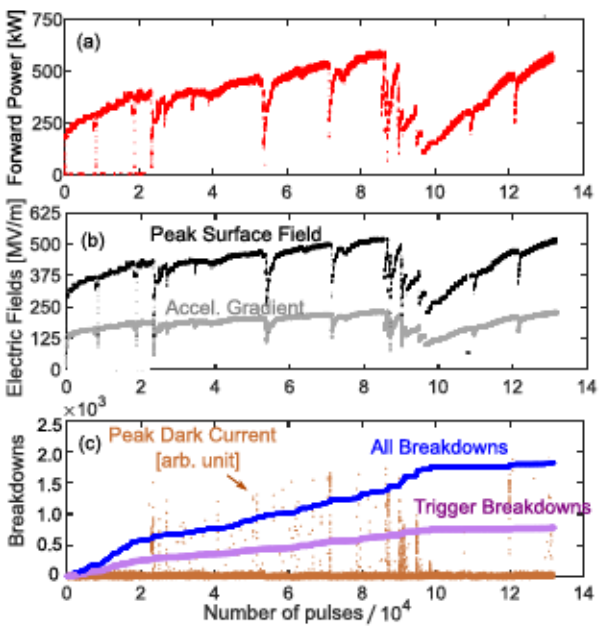

FIG. 4. Timeline of the high gradient processing of the mm-wave accelerating cavity consisting of 1.3×10^5 pulses, showing (a) the forward power, (a) accelerating gradient and peak surface electric field, and (c) number of accumulated breakdowns, trigger breakdowns, and peak breakdown Faraday cup current.

reach 150 MV/m gradient after 10^4 pulses while observing less than 500 breakdowns. Note that we have not observed a current spike during pulse shortening events for gradients less than 150 MV/m. After ramping up the gradient from 100 MV/m to 200 MV/m over the course of 2×10^4 pulses (from 10^5 to 1.2×10^5 in Fig. 4), we have only observed 2 breakdowns and no trigger breakdowns. Moreover, we have not detected currents for pulses with no breakdown up to the highest gradient of 230 MV/m. We have achieved this maximum gradient after 1830 breakdowns in total.

After maintaining that gradient for 3×10^3 consecutive shots, we observed 22 breakdowns with 2 trigger breakdowns. The breakdown rate in the last 10^3 shots at 230 MV/m was about 10^{-3} per pulse. We emphasize that the breakdown rate has not reached a steady state level.

In contrast, a microwave frequency cavity requires millions of pulses to be able to ramp up the gradient. For the sake of comparison, a microwave cavity can only reach a gradient less than 40 MV/m after 10^5 pulses.[31,32] This highlights the potential impact of mm-wave accelerator in terms of rapid conditioning to unprecedented gradients. It is noted also that this first stage of our experiment was limited to 1.5×10^5 pulses at 1 Hz operation and a maximum power of 600 kW. We expect that the breakdown rates will further decrease for extended running time.

In summary, we have presented the experimental measurement of high gradient in a 110 GHz accelerating cavity powered by an external source, a megawatt gyrotron. We have utilized a laser-driven switch to chop nanosecond-scale pulses from 3 μs gyrotron pulses. We coupled 570 kW 10 ns pulses into the cavity and achieved remarkable accelerating gradients up to 230 MV/m. To reach this gradient, the cavity was conditioned with more than 10^5 pulses. We believe that with more conditioning, the breakdown rates will decrease further.

Due to possible imperfections in the joint between the two diffusion-bonded cavity blocks,[42] the peak surface electric fields may exceed 520 MV/m calculated for an ideal cavity surface and may contribute to high breakdowns and field emissions. For this reason, we are exploring new structures assembled with other joining techniques such as brazing and careful surface preparation that may offer better joint quality.[50]

Finally, the rf pulse length may be tuned by deploying other semiconductor wafer materials[44] in the laser-driven switch. Higher peak powers by means of rf pulse compression[51,52] could further push the achievable gradient. This study opens routes toward the use of externally driven high field subterahertz structures not only in future accelerator applications but also in probing material dynamics and inducing nonlinear phenomena.

The authors thank Michael Shapiro, Michelle Gonzalez, Ann Sy, and Gordon Bowden for helpful discussions. We would also like to thank the Fusion Energy Group at General Atomics for equipment loans of quasi-optical equipment that enable low and high-power testing of this structure. This work was supported by the Department of Energy Contract No. DE-AC02-76SF00515 (SLAC) and Grant No. DE-SC0015566 (MIT). This work was also supported by NSF Grant No. PHY-1734015.

DATA AVAILABILITY

The data that support the findings of this study are available from the corresponding author upon reasonable request.

REFERENCES

[1]H. Wiedemann, Part. Accel. Phys. **177**, 541–576 (2007).
[2]E. A. Nanni, W. R. Huang, K.-H. Hong, K. Ravi, A. Fallahi, G. Moriena, R. J. Dwayne Miller, and F. X. Kärtner, Nat. Commun. **6**, 8486 (2015).
[3]D. H. Whittum, "Millimeter-wave drivers for future linear colliders," in 22nd International Conference on Infrared and Millimeter Waves, Wintergreen, USA, 1998, Report No. SLAC-PUB-7809, 1998.
[4]F. Zimmermann, D. H. Whittum, C. K. Ng, and M. E. Hill, AIP Conf. Proc. **472**, 270 (1999).
[5]H. Owen, A. Lomax, and S. Jolly, Nucl. Instrum. Methods Phys. Res., Sect. A **809**, 96 (2016).
[6]T. Ishikawa, H. Aoyagi, T. Asaka, Y. Asano, N. Azumi, T. Bizen, H. Ego, K. Fukami, T. Fukui, and Y. Furukawa, Nat. Photonics **6**, 540 (2012).
[7]A. H. Zewail, Annu. Rev. Phys. Chem. **57**, 65 (2006).
[8]S. P. Weathersby, G. Brown, M. Centurion, T. F. Chase, R. Coffee, J. Corbett, J. P. Eichner, J. C. Frisch, A. R. Fry, and M. Gühr, Rev. Sci. Instrum. **86**, 073702 (2015).
[9]M. Dal Forno, V. Dolgashev, G. Bowden, C. Clarke, M. Hogan, D. McCormick, A. Novokhatski, B. Spataro, S. Weathersby, and S. G. Tantawi, Phys. Rev. Accel. Beams **19**, 051302 (2016).
[10]M. E. Hill, C. Adolphsen, W. Baumgartner, R. S. Callin, X. E. Lin, M. Seidel, T. Slaton, and D. H. Whittum, Phys. Rev. Lett. **87**, 094801 (2001).
[11]M. C. Thompson, H. Badakov, A. M. Cook, J. B. Rosenzweig, R. Tikhoplav, G. Travish, I. Blumenfeld, M. J. Hogan, R. Ischebeck, N. Kirby, R. Siemann, D. Walz, P. Muggli, A. Scott, and R. B. Yoder, Phys. Rev. Lett. **100**, 214801 (2008).
[12]G. Andonian, D. Stratakis, M. Babzien, S. Barber, M. Fedurin, E. Hemsing, K. Kusche, P. Muggli, B. O'Shea, X. Wei, O. Williams, V. Yakimenko, and J. B. Rosenzweig, Phys. Rev. Lett. **108**, 244801 (2012).
[13]S. Antipov, S. V. Baryshev, R. Kostin, S. Baturin, J. Qiu, C. Jing, C. Swinson, M. Fedurin, and D. Wang, Appl. Phys. Lett. **109**, 142901 (2016).
[14]P. J. Chou, G. B. Bowden, M. R. Copeland, A. Farvid, R. E. Kirby, A. Menegat, C. Pearson, L. Shere, R. H. Siemann, J. E. Spencer, and D. H. Whittum, in Seventh Workshop Advanced Accelerator Concepts (ASCE, Lake Tahoe, California USA, 1997), pp. 501–517.
[15]S. S. Dhillon, M. S. Vitiello, E. H. Linfield, A. G. Davies, M. C. Hoffmann, J. Booske, C. Paoloni, M. Gensch, P. Weightman, G. P. Williams, E. Castro-Camus, D. R. S. Cumming, F. Simoens, I. Escorcia-Carranza, J. Grant, S. Lucyszyn, M. Kuwata-Gonokami, K. Konishi, M. Koch, C. A. Schmuttenmaer, T. L. Cocker, R. Huber, A. G. Markelz, Z. D. Taylor, V. P. Wallace, J. A. Zeitler, J. Sibik, T. M. Korter, B. Ellison, S. Rea, P. Goldsmith, K. B. Cooper, R. Appleby, D. Pardo, P. G. Huggard, V. Krozer, H. Shams, M. Fice, C. Renaud, A. Seeds, A. Stöhr, M. Naftaly, N. Ridler, R. Clarke, J. E. Cunningham, and M. B. Johnston, J. Phys. Appl. Phys. **50**, 043001 (2017).
[16]J. Hebling, G. Almási, I. Z. Kozma, and J. Kuhl, Opt. Express **10**, 1161 (2002).
[17]J. Hebling, K.-L. Yeh, M. C. Hoffmann, B. Bartal, and K. A. Nelson, J. Opt. Soc. Am. B **25**, B6 (2008).
[18]W. R. Huang, A. Fallahi, X. Wu, H. Cankaya, A.-L. Calendron, K. Ravi, D. Zhang, E. A. Nanni, K.-H. Hong, and F. X. Kärtner, Optica **3**, 1209 (2016).
[19]R. K. Li, M. C. Hoffmann, E. A. Nanni, S. H. Glenzer, M. E. Kozina, A. M. Lindenberg, B. K. Ofori-Okai, A. H. Reid, X. Shen, S. P. Weathersby, J. Yang, M. Zajac, and X. J. Wang, Phys. Rev. Accel. Beams **22**, 012803 (2019).
[20]D. A. Walsh, D. S. Lake, E. W. Snedden, M. J. Cliffe, D. M. Graham, and S. P. Jamison, Nat. Commun. **8**, 1 (2017).
[21]D. Zhang, A. Fallahi, M. Hemmer, X. Wu, M. Fakhari, Y. Hua, H. Cankaya, A.-L. Calendron, L. E. Zapata, and N. H. Matlis, Nat. Photonics **12**, 336 (2018).
[22]E. Curry, S. Fabbri, J. Maxson, P. Musumeci, and A. Gover, Phys. Rev. Lett. **120**, 094801 (2018).
[23]L. J. Wong, A. Fallahi, and F. X. Kärtner, Opt. Express **21**, 9792 (2013).
[24]E. C. Snively, M. A. K. Othman, M. Kozina, B. K. Ofori-Okai, S. P. Weathersby, S. Park, X. Shen, X. J. Wang, M. C. Hoffmann, R. K. Li, and E. A. Nanni, Phys. Rev. Lett. **124**, 054801 (2020).
[25]L. Zhao, H. Tang, C. Lu, T. Jiang, P. Zhu, L. Hu, W. Song, H. Wang, J. Qiu, C. Jing, S. Antipov, D. Xiang, and J. Zhang, Phys. Rev. Lett. **124**, 054802 (2020).
[26]K. E. Kreischer and R. J. Temkin, Phys. Rev. Lett. **59**, 547 (1987).
[27]W. Hu, M. Shapiro, K. E. Kreischer, and R. J. Temkin, IEEE Trans. Plasma Sci. **26**, 366 (1998).

[28]K. Sakamoto, A. Kasugai, K. Takahashi, R. Minami, N. Kobayashi, and K. Kajiwara, Nat. Phys. **3**, 411 (2007).
[29]D. S. Tax, O. V. Sinitsyn, W. C. Guss, G. S. Nusinovich, M. A. Shapiro, and R. J. Temkin, IEEE Trans. Plasma Sci. **41**, 862 (2013).
[30]A. Grudiev, S. Calatroni, and W. Wuensch, Phys. Rev. Spec. Top.–Accel. Beams **12**, 102001 (2009).
[31]V. Dolgashev, S. Tantawi, Y. Higashi, and B. Spataro, Appl. Phys. Lett. **97**, 171501 (2010).
[32]A. Degiovanni, W. Wuensch, and J. G. Navarro, Phys. Rev. Accel. Beams **19**, 032001 (2016).
[33]V. A. Dolgashev, in Proceedings of the Particle Accelerator Conference (2003), Vol. 2, pp. 1267–1269.
[34]L. Laurent, S. Tantawi, V. Dolgashev, C. Nantista, Y. Higashi, M. Aicheler, S. Heikkinen, and W. Wuensch, Phys. Rev. Spec. Top.–Accel. Beams **14**, 041001 (2011).
[35]K. Nordlund and F. Djurabekova, Phys. Rev. Spec. Top.–Accel. Beams **15**, 071002 (2012).
[36]X. Wu, H. Zha, J. Shi, H. Chen, T. Abe, T. Higo, and S. Matsumoto, Phys. Rev. Accel. Beams **22**, 031001 (2019).
[37]X. Wu, J. Shi, H. Chen, J. Shao, T. Abe, T. Higo, S. Matsumoto, and W. Wuensch, Phys. Rev. Accel. Beams **20**, 052001 (2017).
[38]D. Alesini, M. Bellaveglia, F. Cardelli, R. Di Raddo, A. Gallo, V. Lollo, L. Piersanti, A. Variola, L. Palumbo, F. Poletto, and P. Favaron, Phys. Rev. Accel. Beams **23**, 042001 (2020).
[39]H. Zha and A. Grudiev, Phys. Rev. Accel. Beams **19**, 111003 (2016).
[40]M. Dal Forno, V. Dolgashev, G. Bowden, C. Clarke, M. Hogan, D. McCormick, A. Novokhatski, B. Spataro, S. Weathersby, and S. G. Tantawi, Phys. Rev. Accel. Beams **19**, 011301 (2016).
[41]M. Dal Forno, V. Dolgashev, G. Bowden, C. Clarke, M. Hogan, D. McCormick, A. Novokhatski, B. O'Shea, B. Spataro, S. Weathersby, and S. G. Tantawi, Phys. Rev. Accel. Beams **19**, 111301 (2016).
[42]E. A. Nanni, V. A. Dolgashev, A. Haase, J. Neilson, S. Tantawi, S. C. Schaub, R. J. Temkin, and B. Spataro, J. Phys.: Conf. Ser. **874**, 012039 (2017).
[43]D. S. Tax, B. Y. Rock, B. J. Fox, S. K. Jawla, S. C. Schaub, M. A. Shapiro, R. J. Temkin, and R. J. Vernon, IEEE Trans. Plasma Sci. **42**, 1128 (2014).
[44]J. F. Picard, S. C. Schaub, G. Rosenzweig, J. C. Stephens, M. A. Shapiro, and R. J. Temkin, Appl. Phys. Lett. **114**, 164102 (2019).
[45]S. V. Kutsaev, B. Jacobson, A. Y. Smirnov, T. Campese, V. A. Dolgashev, V. Goncharik, M. Harrison, A. Murokh, E. Nanni, J. Picard, M. Ruelas, and S. C. Schaub, Phys. Rev. Appl. **11**, 034052 (2019).
[46]T. Vogel, G. Dodel, E. Holzhauer, H. Salzmann, and A. Theurer, Appl. Opt. **31**, 329 (1992).
[47]M. L. Kulygin, G. G. Denisov, and V. V. Kocharovsky, J. Infrared, Millimeter, Terahertz Waves **31**, 31–40 (2009).
[48]P. B. Wilson, AIP Conf. Proc. **24**, 191 (1997).
[49]A. D. Cahill, J. B. Rosenzweig, V. A. Dolgashev, S. G. Tantawi, and S. Weathersby, Phys. Rev. Accel. Beams **21**, 102002 (2018).
[50]M. Othman, B. Angier, A. Haase, E. Nanni, M. Roux, and A. Sy, Proceedings of the 10th International Particle Accelerator Conference IPAC2019, Australia (2019), pp. 3764–3765.
[51]M. Petelin, V. Erckmann, J. Hirshfield, W. Kasparek, D. Shchegolkov, and A. Tolkachev, IEEE Trans. Electron Devices **56**, 835 (2009).
[52]L. Zhang, S. V. Mishakin, W. He, S. V. Samsonov, M. McStravick, G. G. Denisov, A. W. Cross, V. L. Bratman, C. G. Whyte, C. W. Robertson, A. R. Young, K. Ronald, and A. D. R. Phelps, IEEE Trans. Microwave Theory Tech. **63**, 1090 (2015).